Journal of Computational Physics 229 (2010) 2497–2506

Contents lists available at ScienceDirect

Journal of Computational Physics

journal homepage: www.elsevier.com/locate/jcp

# Momentum transfer correction for macroscopic-gradient boundary conditions in lattice Boltzmann methods

Salvador Izquierdo, Norberto Fueyo *

*Laboratorio de Investigación en Tecnologías de la Combustión (LITEC), Centro Superior de Investigaciones Científicas (CSIC), María de Luna 10, 50018 Zaragoza, Spain*
*Fluid Mechanics Group, University of Zaragoza, María de Luna 3, 50018 Zaragoza, Spain*

ARTICLE INFO

*Article history:*
Received 12 March 2009
Received in revised form 2 November 2009
Accepted 25 November 2009
Available online 16 December 2009

*Keywords:*
Computational fluid dynamics
Lattice Boltzmann
Momentum boundary conditions
Neumann boundary condition
Robin boundary condition
Walls

ABSTRACT

The boundary conditions used to represent macroscopic-gradient-related effects in arbitrary geometries with the lattice Boltzmann methods need a trade-off between the complexity of the scheme, due to the loss of localness and the difficulties for directly applying link-based approaches, and the accuracy obtained. A generalization of the momentum transfer boundary condition is presented, in which the arbitrary location of the boundary is addressed with link-wise interpolation (used for Dirichlet conditions) and the macroscopic gradient is taken into account with a finite-difference scheme. This leads to a stable approach for arbitrary geometries that can be used to impose Neumann and Robin boundary conditions. The proposal is validated for stress boundary conditions at walls. Two-dimensional steady and unsteady configurations are used as test case: partial-slip flow between two infinite plates and the slip flow past a circular cylinder.

© 2009 Elsevier Inc. All rights reserved.

## 1. Introduction

Lattice Boltzmann (LB) methods [1–4] are an efficient approach to simulate fluid flow based on the solution of the Boltzmann equation with a minimal discretization of the velocity space [5]. One of its strengths is the ability to simulate complex geometries with little additional computational effort. Simulations with detailed geometries of porous media [6], blood vessels [7], indoor environments [8] or flow aerodynamics [9] are some successful examples. Different implementations of Dirichlet conditions for arbitrary geometries have been developed; however, little research has been published related to the implementation of Neumann boundary conditions. This deficit is probably due to several factors, which can be illustrated using the stress boundary-condition as an example. First, the stresses are macroscopic moments related to the non-equilibrium part of the distribution functions that have an $O(\partial_j u_i)$ influence on the accuracy of the boundary condition, which is sometimes neglected; additionally, many configurations do not require these kind of boundary conditions, and in the most common case where it is needed (i.e. zero tangential stresses for symmetry planes) the link-based approach can be applied through a specular reflection; furthermore, it is a hydrodynamic boundary condition, and kinetic ones are often preferred (especially for microflows). The use of Neumann conditions would allow to extend the applicability of the lattice Boltzmann method by prescribing, for example, effects related to $\partial_j u_i$ (e.g. stress over a porous wall, wall models for turbulent flows, hydrophobic-hydrophilic wall treatments) and to reduce the complexity of the domain (e.g. symmetry axis).

In the following, the evolution of the implementation of boundary conditions in lattice Boltzmann methods is reviewed to serve as a basis for the evaluation of the best way to implement Neumann conditions. In this discussion, only macroscopic boundary conditions for the momentum equations are considered. However, the conclusions presented can be extended to any other macroscopic variable.

* Corresponding author. Tel.: +34 976762153; fax: +34 976761882.
*E-mail addresses:* Salvador.Izquierdo@unizar.es (S. Izquierdo), Norberto.Fueyo@unizar.es (N. Fueyo).

0021-9991/$ - see front matter © 2009 Elsevier Inc. All rights reserved.
doi:10.1016/j.jcp.2009.11.036

The first approach to model walls in LB is the use of the bounce-back scheme (see, for example, [10]) for the non-slip condition, and the application of a specular reflection for the complete slip or zero-stress one. From this straightforward approach it is possible to observe the obvious relationship between the stress at the wall, the wall collision, and the slip condition.

With the bounce-back scheme as the starting point, two pieces of work elaborated on improved boundary conditions for LB. One of them established the influence of the relaxation parameters on the wall location [11] and the other studied the influence of the definition of the non-equilibrium part of the distribution functions on wall (and initial) conditions [12]. Also relevant to the present discussion are some further papers describing alternative approaches to improve the accuracy of the bounce-back boundary condition considering different lattices (e.g. [13–16]).

A first work on including arbitrary geometries was the one by Ginzbourg and d'Humières [17] for a Poiseuille flow in inclined channels. Filippova and Hänel [18] developed an approach for dealing with complex geometries based on modifications to the bounce-back procedure using interpolation; this approach was improved by Mei et al. [19] and [20], and generalized by Ginzburg et al. [21,22]. Another approach to simulate curved geometries is based on the volumetric scheme by Chen et al. [23], that has also been improved upon [24]. The work by Verberg and Ladd [25] can be considered a different way to impose volumetric boundary conditions. One further approach is the extrapolation proposed by Chen et al. [26] and extended to curved geometries by Guo et al. [27]. Two additional concepts have been introduced, related to local boundary conditions [17,28,29], and immersed boundary conditions for lattice Boltzmann methods [30].

The development of Neumann boundary treatments in LB largely focuses on the definition of slip boundaries, or stress-related conditions, as they are linked to the development of wall boundary-conditions for microflows [31–33]. Although the use of kinetic boundary conditions to impose a pre-defined stresses has been attempted for planar walls, no satisfactory result has been obtained in curved geometries, for which their application becomes complex or impossible [32,34].

Some attempts to simulate configurations which need Neumann conditions can be found in the literature [35,34]. The best-suited hydrodynamic approach for setting Neumann conditions at boundaries, even with complex geometries, is often claimed to be the volumetric approach by Chen et al. [23].

The preceding review of boundary conditions for lattice Boltzmann methods provide some guidelines for an efficient implementation of Neumann boundary conditions. Thus, any method proposed should: (i) preserve the simplicity and good stability behavior of bounce-back-based schemes; (ii) be second-order (or higher) for arbitrary geometries; (iii) avoid the use of extrapolations related to hydrodynamic treatments [26]; and (iv) avoid the use of non-lattice distribution functions as in kinetic methods with non-zero off-diagonal kernels [31,36].

The approach presented here treats the problem in a general efficient way preserving well-established boundary treatments [22] and including macroscopic-gradients with a low degree of added complexity. It is a practical approximation to solve the problem that can be formulated in a modular way to introduce improvements that do not change the basic structure.

The paper is organized as follows. Section 2 briefly describes the multi-relaxation-times (MRT) lattice Boltzmann method used to test the boundary treatment proposed. In Section 3 the implementation of gradient-based boundary conditions is introduced. In Section 4 results for different test cases are presented. Finally, (Section 5), some conclusions from the results and an outline of possible applications are discussed.

## 2. The lattice Boltzmann method

The approach to boundary treatment presented in this paper is independent of the lattice Boltzmann method used. However, we choose an MRT lattice Boltzmann method [37] because the access to a larger number of relaxation factors allows to improve the stability of the method, and to influence the accuracy of the boundary conditions.

A two dimensional (D2Q9) method with nine velocities $\mathbf{e}_i = (e_{x\alpha}, e_{y\alpha})$ with $e_{x\alpha} = (0,1,0,-1,0,1,-1,-1,1)$ and $e_{y\alpha} = (0,0,1,0,-1,1,1,-1,-1)$, is used. The velocity distribution functions $\mathbf{f} \equiv f_\alpha \in \mathbb{R}^9$ evolve according to nine velocities in a two dimensional lattice of nodes $x_i \in \mathbb{Z}^2$. The evolution equation for $\mathbf{f}$ is:

$$\mathbf{f}(x_i + \mathbf{e}_i\delta t, t+\delta t) - \mathbf{f}(x_i,t) = -\mathbf{M}^{-1}\cdot\mathbf{S}\cdot[\mathbf{m}(x_i,t) - \mathbf{m}^{eq}(x_i,t)] + \mathbf{F}(x_i,t); \tag{1}$$

where the lower-case-bold symbols, $\mathbf{f}$ and $\mathbf{m}$, denote transpose 9-dimensional vectors; $\mathbf{M}$ is the transformation matrix that linearly relates velocity distribution functions and moments: $\mathbf{f} = \mathbf{M}^{-1}\cdot\mathbf{m}$ and $\mathbf{m} = \mathbf{M}\cdot\mathbf{f}$; $\mathbf{m} = (\rho, e, \epsilon, \rho u_x, q_x, \rho u_y, q_y, p_{xx}, p_{xy})^T$ are the macroscopic moments and $\mathbf{m}^{eq}$ their equilibrium values; $\mathbf{S} = \mathrm{diag}(0, s_e, s_\epsilon, 0, s_\alpha, 0, s_\alpha, s_v, s_v)$ is a diagonal matrix of relaxation factors, where $s_v$ is related to the viscosity; $c_s$ is the speed of sound, and $w_\alpha = (4/9, 1/9, 1/9, 1/9, 1/9, 1/36, 1/36, 1/36, 1/36)$ are the weighting coefficients for each velocity. $\mathbf{F} \equiv F_\alpha = 1/c_s^2 w_\alpha \rho_0 \delta t(e_{i\alpha}a_i)$ is an external body force, $a_i$ being the acceleration induced by this force. Additional details about the definition of body forces and their influence on momentum are discussed, for example, in [38]. Further information about the method can be found in the work by Lallemand and Luo [39]. Essentially, we work with a simplified version of the MRT collision operator with only two relaxation times (TRT) [40–43,22,44]. For this case $s_e = s_\epsilon = s_v$ and $s_\alpha$ is related to $s_v$ in order to reduce errors at the boundary in a way which varies depending on the interpolation scheme used. Unless otherwise indicated, we will take $s_\alpha = 8(2-s_v)/(8-s_v)$ [21,22].

Applying a Chapman-Enskog expansion to Eq. (1) the Navier–Stokes equations are recovered in the limit of low $Kn$ and low $Ma$ numbers, with $\rho = \sum_\alpha f_\alpha$ and $\rho u_i = \sum_\alpha (e_{i\alpha}f_\alpha) + F_i/2$. The fluid viscosity is related to $s_v$ as: $\nu = c_s^2(1/s_v - 1/2)$. A speed of sound $c_s = 1/\sqrt{3}$ is considered hereafter.

## 3. Gradient-based boundary conditions

Following the desirable properties detailed above, the present proposal is based on: (i) An interpolation scheme to set Dirichlet boundary-conditions for arbitrary walls. For first- and second-order approximations the scheme by Bouzidi et al. [20] can be applied. For higher-order approximations the multireflection boundary condition by Ginzburg and d'Humières [21] should be used. For a generalized approach the work by Ginzburg et al. [22] can be consulted. (ii) A pre-defined stencil for the derivative of the macroscopic variable. The stencil can use non-lattice values obtained by interpolating macroscopic quantities computed on the lattice.

This boundary treatment is described in the following for velocity-gradient conditions. The terminology by Ginzburg et al. [22] is followed to define the different interpolation schemes applied.

Some definitions, used to simplify the description of these schemes, are introduced next. The equilibrium distribution function can be split in a symmetric:

$$f_\alpha^{eq+} = \omega_\alpha \rho + \frac{9}{2}\omega_\alpha \rho_0 \left[ (\mathbf{e}_\alpha \cdot \mathbf{u})^2 - \frac{1}{3}(\mathbf{u}\cdot\mathbf{u}) \right]; \tag{2}$$

and an anti-symmetric part:

$$f_\alpha^{eq-} = 3\omega_\alpha \rho_0 (\mathbf{e}_\alpha \cdot \mathbf{u}). \tag{3}$$

A similar description is used for distribution functions $f_\alpha = f_\alpha^+ + f_\alpha^-$, the components of which are defined as:

$$f_\alpha^+ = \frac{1}{2}(f_\alpha + f_{\bar\alpha}), \tag{4}$$

$$f_\alpha^- = \frac{1}{2}(f_\alpha - f_{\bar\alpha}); \tag{5}$$

where $\bar\alpha$ is the direction opposite to $\alpha$ in a link.

The non-equilibrium distribution function are then computed as:

$$f_\alpha^{neq+} = f_\alpha^+ - f_\alpha^{eq+}; \tag{6}$$

$$f_\alpha^{neq-} = f_\alpha^- - f_\alpha^{eq-}. \tag{7}$$

### 3.1. Velocity-gradient boundary condition

The distribution function in Dirichlet-velocity boundaries (see Fig. 1) can be generically computed through three terms [22]:

$$f_{\bar\alpha}(\mathbf{x}_f, t+1) = R_\alpha^{(u)}(\mathbf{x}_f, t) + F_\alpha^{p.c.(u)}(\mathbf{x}_f, t) + W_\alpha^{(u)}(\mathbf{x}_b, \hat t); \tag{8}$$

where $R_\alpha^{(u)}(\mathbf{x}_f, t)$ is the interpolation scheme, $F_\alpha^{p.c.(u)}(\mathbf{x}_f, t)$ is the error correction to match the desired accuracy derived from a Chapman-Enskog expansion, and $W_\alpha^{(u)}(\mathbf{x}_b, \hat t)$ is the Dirichlet condition at the boundary $\mathbf{x}_b$ and at a time $\hat t = t + \Delta t$, which depends on the interpolation scheme applied. The time $\hat t$ is the most appropriate time (after theoretical and numerical analysis of the boundary condition [22]) to impose a time-dependent boundary condition. Three interpolation schemes among the possible ones are described next for completeness.

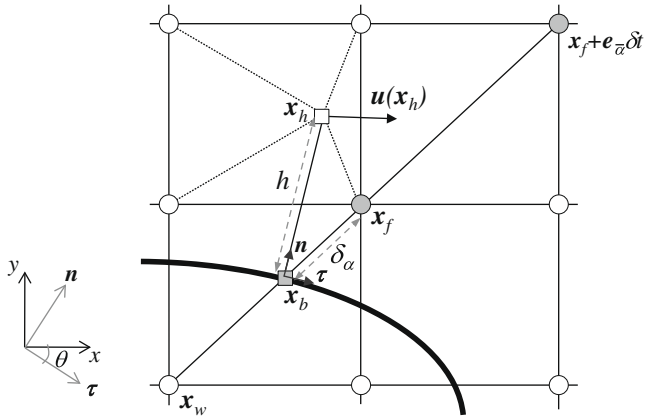


**Fig. 1.** Schematic view of the wall treatment including generic reference axis at the wall.

*3.1.1. Velocity bounce-back (BB)*

The BB is the simplest scheme with the following terms:

$$R_\alpha^{(u)}(\mathbf{x}_f,t)=\tilde{f}_\alpha(\mathbf{x}_f,t); \tag{9a}$$

$$F_\alpha^{p.c.(u)}(\mathbf{x}_f,t)=0; \tag{9b}$$

$$W_\alpha^{(u)}(\mathbf{x}_b,\hat{t})=-2f_\alpha^{eq-}(\mathbf{x}_b,\hat{t}); \tag{9c}$$

where $\tilde{f}$ are post-collision distribution functions. For these cases $\delta_\alpha=1/2$ for every boundary link, where $\delta_\alpha$ is defined as $\delta_\alpha=|\mathbf{x}_f-\mathbf{x}_b|/|\mathbf{x}_f-\mathbf{x}_w|$ (see Fig. 1); $\hat{t}=t+1/2$; and the accuracy obtained is second order for the anti-symmetric part of the distribution function (referred to as $u^{(2)}$), and first order for the symmetric part (referred to as $\Pi^{(1)}$).

*3.1.2. Upwind/downwind linear interpolation (ULI/DLI)*

The accuracy obtained with ULI/DLI is $u^{(2)}$ and $\Pi^{(1)}$. The ULI [20,22] is used for $0\leqslant\delta_\alpha\leqslant 1/2$:

$$R_\alpha^{(u)}(\mathbf{x}_f,t)=2\delta_\alpha\tilde{f}_\alpha(\mathbf{x}_f,t)+(1-2\delta_\alpha)\tilde{f}_\alpha(\mathbf{x}_f+\mathbf{e}_\alpha\delta t,t); \tag{10a}$$

$$F_\alpha^{p.c.(u)}(\mathbf{x}_f,t)=0; \tag{10b}$$

$$W_\alpha^{(u)}(\mathbf{x}_b,\hat{t})=-2f_\alpha^{eq-}(\mathbf{x}_b,\hat{t}); \tag{10c}$$

with $\hat{t}=t+(1-\delta_\alpha)$.

The DLI [20,22] is used for $\delta_\alpha\geqslant 1/2$:

$$R_\alpha^{(u)}(\mathbf{x}_f,t)=\frac{1}{2\delta_\alpha}\tilde{f}_\alpha(\mathbf{x}_f,t)+\frac{2\delta_\alpha-1}{2\delta_\alpha}\tilde{f}_{\bar{\alpha}}(\mathbf{x}_f,t); \tag{11a}$$

$$F_\alpha^{p.c.(u)}(\mathbf{x}_f,t)=0; \tag{11b}$$

$$W_\alpha^{(u)}(\mathbf{x}_b,\hat{t})=-\frac{1}{\delta_\alpha}f_\alpha^{eq-}(\mathbf{x}_b,\hat{t}); \tag{11c}$$

with $\hat{t}=t+\delta_\alpha$.

*3.1.3. Improved upwind/downwind linear interpolation (MGULI/MGDLI)*

The MGULI/MGDLI is and improved ULI/DLI interpolation where $O(u)$ errors are canceled through the $F_\alpha^{p.c.(u)}$ term. $R_\alpha^{(u)}, W_\alpha^{(u)}, \hat{t}$ and the ranges of applicability with regard to $\delta_\alpha$ remain as in ULI/DLI. For MGULI the corresponding correction term reads:

$$F_\alpha^{p.c.(u)}(\mathbf{x}_f,t)=-4\left(\delta_\alpha-\frac{1}{2}\right)\left(1-\frac{1}{s_\alpha}\right); \tag{12}$$

and for MGDLI it is:

$$F_\alpha^{p.c.(u)}(\mathbf{x}_f,t)=-\frac{2}{\delta_\alpha}\left(\frac{1}{2}-\delta_\alpha\right)\left(\frac{1-\delta_\alpha}{\delta_\alpha}-\frac{1}{2s_\alpha\delta_\alpha}\right); \tag{13}$$

This correction can be further improved by equalizing $O(u^2)$ errors, leading to the MULI/MDLI scheme proposed in [22].

*3.1.4. Derivative stencils*

Velocity-gradient boundary conditions for the Navier–Stokes equations are directly related to the stress tensor, which in two-dimensions is:

$$\sigma_{ij}=\begin{pmatrix}\sigma_{nn} & \sigma_{n\tau}\\ \sigma_{\tau n} & \sigma_{\tau\tau}\end{pmatrix}=\begin{pmatrix}\rho_0\nu\frac{\partial u_n}{\partial n}-p & \rho_0\nu\frac{\partial u_\tau}{\partial n}\\ \rho_0\nu\frac{\partial u_n}{\partial \tau} & \rho_0\nu\frac{\partial u_\tau}{\partial \tau}-p\end{pmatrix}. \tag{14}$$

When imposing Neumann or Robin conditions for the velocity at the boundaries special attention must be paid to ensure that the full stress tensor is defined, including the pressure terms. In this work, Neumann and Robin conditions will be applied to impervious walls (not in open boundaries) for two dimensional incompressible flows. Thus, only $\sigma_{n\tau}$ is relevant. For a complete description of the initial and boundary value problem for the Navier–Stokes equations we refer to [45].

The finite-difference-derivative stencils for the velocity needed for computing the stress at walls are obtained from a Taylor series expansion of the velocity around two points in the direction normal to the wall. Let these points be located at a distance $h_1$ and $h_2$ from a boundary point $\mathbf{x}_b$; then, from a Taylor expansion up to the second order in $h_1$ and $h_2$:

$$u_\tau(\mathbf{x}_b+h_1)=u_\tau(\mathbf{x}_b)+h_1\frac{\partial u_\tau}{\partial n}(\mathbf{x}_b)+\frac{h_1^2}{2}\frac{\partial^2 u_\tau}{\partial n^2}(\mathbf{x}_b)+O(h_1^3); \tag{15a}$$

$$u_\tau(\mathbf{x}_b+h_2)=u_\tau(\mathbf{x}_b)+h_2\frac{\partial u_\tau}{\partial n}(\mathbf{x}_b)+\frac{h_2^2}{2}\frac{\partial^2 u_\tau}{\partial n^2}(\mathbf{x}_b)+O(h_2^3); \tag{15b}$$

we can obtain expressions for the first and second-order derivatives:

$$\frac{\partial u_\tau}{\partial n}(\mathbf{x}_b) \approx \frac{h_1^2[u_\tau(\mathbf{x}_b) - u_\tau(\mathbf{x}_{h_2})] + h_2^2[u_\tau(\mathbf{x}_{h_1}) - u_\tau(\mathbf{x}_b)]}{h_1 h_2 (h_2 - h_1)}; \tag{16a}$$

$$\frac{\partial^2 u_\tau}{\partial n^2}(\mathbf{x}_b) \approx \frac{2h_1[u_\tau(\mathbf{x}_{h_2}) - u_\tau(\mathbf{x}_b)] + 2h_2[u_\tau(\mathbf{x}_b) - u_\tau(\mathbf{x}_{h_1})]}{h_1 h_2 (h_2 - h_1)}; \tag{16b}$$

In this work, this approach is simplified by employing a first order stencil for the derivative of the wall-tangential velocity $u_\tau$ along the normal direction $n$. It is considered for this case that $h_1 = h$ is the only point in the normal direction used to compute the tangential stress (see Fig. 1 for nomenclature):

$$\sigma_{n\tau}(\mathbf{x}_b) = \rho_0 \nu \frac{\partial u_\tau}{\partial n}(\mathbf{x}_b) \approx \rho_0 \nu \frac{u_\tau(\mathbf{x}_h) - u_\tau(\mathbf{x}_b)}{h}; \tag{17}$$

where $h = \delta x$ for $\delta_\alpha < 0.5$ and $h = 1.5\delta x\ \delta_\alpha \geqslant 0.5$. This is a somewhat arbitrary selection of $h$ but it allows to compute $u_\tau(\mathbf{x}_h)$ within a region next to the wall where stable interpolation schemes can be applied. A bilinear interpolation of macroscopic variables is used in this work because higher-order interpolations are not expected to generate better or more stable results [46], and because other mixed interpolation techniques used in immersed boundary methods for the Navier–Stokes equations increase the complexity of the implementation [47]. The length $h$ and the corresponding weights for the bilinear interpolation can be computed in a preprocessing, as it is usually done for $\delta_\alpha$ values. This preprocessing is performed only once for stationary geometries.

The first order approximation assumes a linear profile of the stress, which makes it applicable to laminar flows and to turbulent ones with enough resolution near the wall. Wherever this assumption is no longer valid (e.g. non-newtonian fluids), higher-order stencils can be considered. Furthermore, for some special cases (e.g. turbulent flows with coarse near-wall resolution [48] or even for microflows [49]) pre-defined velocity profiles, the so called *wall laws*, can be applied.

For the case of a Neumann boundary condition the velocity to be added to the wall to account for the imposed stresses, considering Eq. (17), is:

$$\rho_0 \nu \frac{\partial u_\tau}{\partial n}(\mathbf{x}_b) = \sigma_{n\tau}(\mathbf{x}_b) \Rightarrow u_\tau(\mathbf{x}_b) \approx u_\tau(\mathbf{x}_h) - \frac{h\sigma_{n\tau}(\mathbf{x}_b)}{\rho_0 \nu}. \tag{18}$$

When a Robin condition is applied, the equivalent wall-slip velocity is computed as:

$$u_\tau(\mathbf{x}_b) = K \frac{\partial u_\tau}{\partial n}(\mathbf{x}_b) \Rightarrow u_\tau(\mathbf{x}_b) \approx \frac{u_\tau(\mathbf{x}_h)}{1 + \frac{h}{KH}}. \tag{19}$$

Finally, to introduce $u_\tau(\mathbf{x}_b)$ into the momentum transfer correction equations, i.e. the Dirichlet term in Eq. (8), a change of coordinates (by rotation) from ($\tau$,n) to (x,y) is needed:

$$\mathbf{u}(\mathbf{x}_b) = (u_x(\mathbf{x}_b), u_y(\mathbf{x}_b)) = u_\tau(\mathbf{x}_b)\boldsymbol{\tau}; \tag{20}$$

where $\boldsymbol{\tau} = (cos\,\theta, -sin\,\theta)$ according to coordinate systems in Fig. 1.

### 3.2. Corners and special boundaries

The term special boundaries is used here to refer to those which do not allow us to properly implement the boundary condition desired. As this depends on the type of boundary condition, different considerations must be made for the macroscopic-gradient-based conditions.

Since in the proposal presented above link-based schemes are applied to take into account arbitrary geometries, the same considerations as in [22] can be made with links where not enough nodes are available in the link direction. If only nodes up to $\mathbf{x}_f + \mathbf{e}_{\bar{\alpha}}\delta t$ are available, $\tilde{f}_\alpha(\mathbf{x}_f + 2\mathbf{e}_{\bar{\alpha}}\delta t, t)$ can be replaced with $f_\alpha(\mathbf{x}_f + \mathbf{e}_{\bar{\alpha}}\delta t, t+1)$. If only $\mathbf{x}_f$ is available, it is possible to switch to BB; or, if $\tilde{f}_\alpha(\mathbf{x}_f + \mathbf{e}_{\bar{\alpha}}\delta t, t)$ is replaced with $f_\alpha(\mathbf{x}_f, t+1)$, it is possible to switch to ULI/DLI. For corners, the bisectrix can be used as the normal direction.

## 4. Test cases

Two test cases are used to validate the proposed new boundary-condition treatment: (i) the flow between two plates with a partial-slip boundary-condition at walls, for both a Couette flow and a laminar channel; and (ii) the flow around a circular cylinder with complete slip at walls. These test cases thus encompass the behavior in steady and unsteady flows, and with planar and curved boundaries. Additionally, the evaluation of forces on objects is tested.

### 4.1. Flow between two plates with partial slip

The laminar two-dimensional steady state flow between two plates located at $y = 0$ and $y = H$ is defined by the Navier–Stokes equations without temporal or convective terms:

$$0 = -\frac{\partial p}{\partial x} + \frac{\partial}{\partial y}\left(\rho_0 \nu \frac{\partial u}{\partial y}\right); \tag{21a}$$

$$0 = \frac{\partial p}{\partial y}. \tag{21b}$$

These equations are solved analytically for two different flows, i.e. Couette and Hagen-Poiseuille, with partial-slip boundary-conditions.

#### 4.1.1. Partial-slip Couette-flow

A Couette flow parallel to the $x$-axis is simulated, where the upper wall drives the flow with $u(H) = u_0$ and the lower wall has a slip behavior defined by two alternative laws: Neumann, $\rho_0 \nu \partial_y u_N(0) = \sigma_{yx}(\mathbf{x}_b)$; and Robin, $u_R(0) = KH\partial_y u(\mathbf{x}_b)$ . The BB boundary condition Eq. (9c) is used for both walls, and periodic conditions are applied at the inlet and at the outlet. Solving Eq. (21b) with these boundary conditions, the following solutions are obtained for the Neumann condition:

$$u_N(y) = u_0 - \frac{\sigma_{yx}(\mathbf{x}_b)}{\rho_0 \nu}(H - y); \tag{22}$$

and for the Robin one:

$$u_R(y) = \frac{u_0(HK + y)}{H + HK}. \tag{23}$$

The respective slip velocities $u_s$ at the lower wall for both conditions are:

$$u_s = u_N(0) = u_0 - \frac{H\sigma_{yx}(\mathbf{x}_b)}{\rho_0 \nu}; \quad u_s = u_R(0) = \frac{u_0 HK}{H + HK}. \tag{24}$$

Simulations to reproduce several slip velocities $u_s$ at the lower wall are performed. The parameters for the Neumann and Robin boundary conditions are computed from Eq. (24) for $u_s = 0, 1/3, 2/3$ and 1. Results are plotted using normalized variables in Fig. 2, where they are also compared with the analytical solution Eqs. (22) and (23).

To validate the behavior of the boundary condition for unsteady simulations the time-dependent equation is solved for the Couette flow with the boundary condition $\sigma_{yx}(\mathbf{x}_b) = 0$ at the lower wall. A Laplace transform procedure is applied (see, for example, [50]) to obtain the analytical solution:

$$u(y,t) = u_0 - \frac{4u_0}{\pi}\sum_{n=0}^{\infty}\frac{(-1)^n}{2n+1} exp\left(-\frac{(2n+1)^2\pi^2}{4}\frac{\nu t}{H^2}\right) \times cos\frac{(2n+1)\pi y}{2H}; \tag{25}$$

where the series are computed up to the $n = 1000$th term to compare with the lattice Boltzmann results. The comparison is shown in Fig. 3, for several dimensionless times $T = \nu t/H^2$. It can be seen that an increment in spatial resolution has a positive effect on the accuracy.

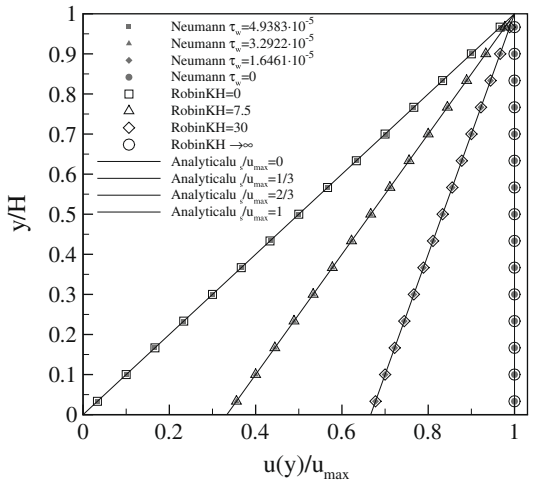


**Fig. 2.** Solutions of the Couette flow for several values of the Robin and Neumann boundary conditions. $Re = 10,\ s_v = 5/3,\ H = 15\delta x$ and $\delta_\alpha = 0.5$.

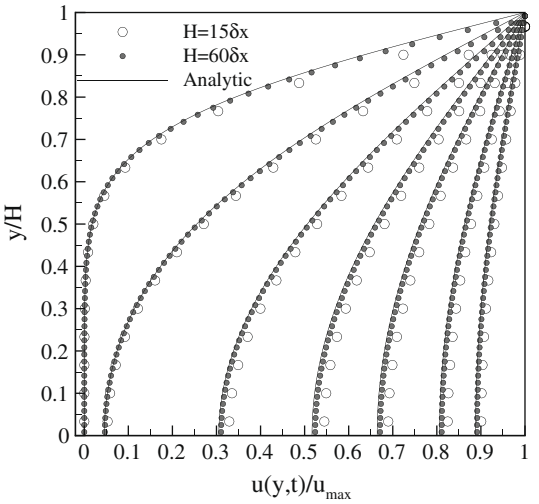


**Fig. 3.** Temporal evolution towards the steady state. $Re = 10,\ s_v = 5/3,\ H = 15\delta x, 60\delta x$ and $\delta_\alpha = 0.5$. From left to right results for $T = 0.022$, 0.096, 0.244, 0.393, 0.541, 0.763 and 0.985. The solid lines are the analytical solutions from Eq. (25).

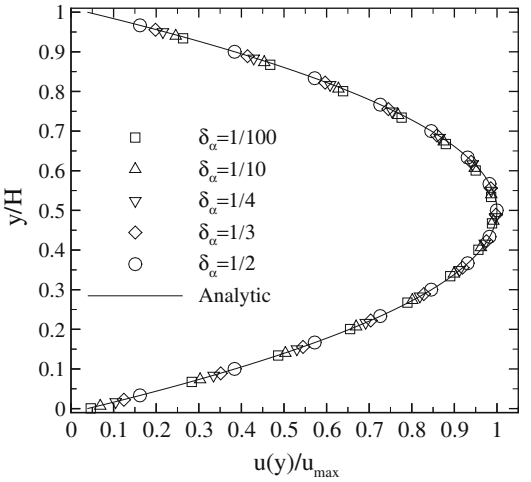


**Fig. 4.** Velocity profile in the slip channel with $K = 0.01$ for several $\delta_\alpha$ in the lower wall. $Re = 10,\ s_v = 5/3$ and $H = 15\delta x$ (ULI/DLI interpolation scheme).

*4.1.2. Partial-slip channel*

The laminar flow in a two-dimensional channel with partial-slip conditions is simulated. Eq. (21b) is solved here using a Robin condition in the lower and upper wall, $u(0) = u(H) = KH\partial_y u$, and with stream-wise periodic conditions. The analytical solution is:

$$u_{max} = -\frac{1}{8\rho_0 \nu}\frac{dp}{dx}H^2(1+4K); \tag{26a}$$

$$u(y) = u_{max}\frac{4(H^2K + Hy - y^2)}{H^2(1+4K)}. \tag{26b}$$

In this case, the BB, ULI/DLI and MGULI/MGDLI schemes are used, with a first order stencil for the velocity derivative. The flow is driven by a body force where the acceleration $dp/dx$ is computed from Eq. (26a) for a prescribed Reynolds number based on $u_{max}$. The ULI/DLI and MGULI/MGDLI schemes allows to evaluate the behavior of the Robin condition for different $\delta_\alpha$ values. In Fig. 4 the velocity profile for several $\delta_\alpha$ in the lower wall is shown (which implies $1 - \delta_\alpha$ in the upper one, as the walls are parallel to the lattice), and compared with the analytical solution for the ULI/DLI scheme.

To test the influence of the interpolation scheme, the error obtained is plotted in Fig. 5 for the simulation of the channel by applying BB, ULI/DLI and MGULI/MGDLI as described in Section 3.1. As a further improved interpolation scheme is used, the effect of $\delta_\alpha$ in the error obtained is reduced (see Fig. 5 (left) ). The second-order approach for the velocity derivatives at

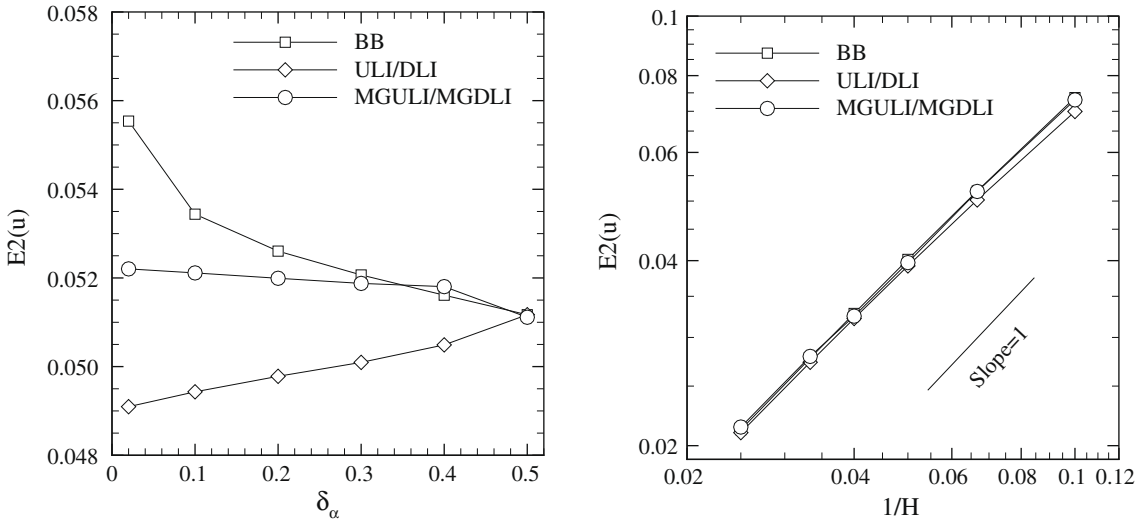


**Fig. 5.** $L_2$-norm error of the velocity for BB, ULI/DLI and MGULI/MGDLI as a function of $\delta_\alpha$ (left) for $Re = 10,\ s_v = 5/3,\ K = 0.01$ and $H = 15\delta x$; and resolution (right) for a constant grid Reynolds number $Re_x = 0.1,\ s_v = 5/3,\ u_{max} = 1/30,\ K = 0.01$ and $\delta_\alpha = 1/2$.

the wall was also tested to numerically verify that for this flow it has no influence on the result. In Fig. 5 (right) it is observed that all three methods exhibit a first-order accuracy; although second-order accuracy was expected for ULI/DLI and MGULI/MGDLI, the implementation of the periodic boundary conditions together with the simplified driving force lead to first order spatial convergence. Nevertheless, the positive feature of avoiding the effect of $\delta_\alpha$ on the solution is preserved. A more detailed study of the accuracy of the method for this flow, as performed in [44], should include inlet and outlet boundary conditions of the same order of accuracy as those used at the walls. Further details on the accuracy of these interpolation schemes can be found in [22].

### 4.2. Slip flow past a cylinder

The two-dimensional flow around a circular cylinder with slip boundary conditions ($\sigma_{n\tau} = 0$) is used to validate the scheme proposed to account for curved boundaries. For this validation the following definition of the drag coefficient is used:

$$C_d = \frac{F_d}{\frac{1}{2}\rho_0 u_0^2 D}. \tag{27}$$

The analytical and experimental expressions to validate the boundary condition proposed in this work are for the low-Reynolds and low-Eotvos number regimes [51], which prevail, for instance, in the slow motion of bubbles in a liquid. An analytical analysis allows to recover the following expressions for very low Reynolds:

$$C_d = \frac{16}{Re}, \tag{28}$$

which is the drag coefficient for the Stokes flow [51]; and

$$C_d = \frac{16}{Re}\left(1 + \frac{Re}{8}\right), \tag{29}$$

which is the Oseen correction for finite Reynolds [51]. For moderate Reynolds numbers $Re > 2$, the following expression can be used [51]:

$$C_d = 14.9 Re^{-0.78}; \tag{30}$$

and for high Reynolds numbers ($Re \gg 1$) the Moore drag estimate is [51]:

$$C_d = \frac{48}{Re}\left[1 - \frac{2.21}{Re^{1/2}}\right]. \tag{31}$$

The main characteristic of the flow around a cylinder or a sphere with total slip at boundaries is the absence of a recirculation region downstream. The calculated flow around a two-dimensional cylinder is represented in Fig. 6, where streamlines and

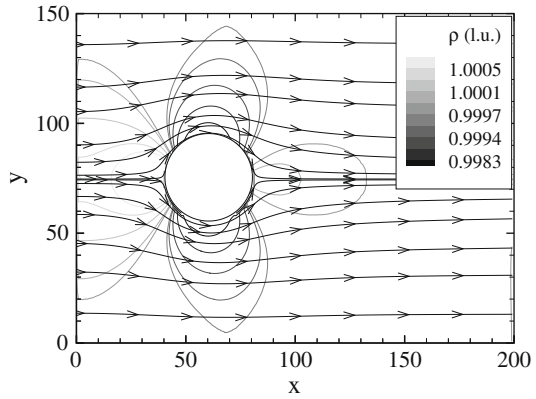


**Fig. 6.** Pressure contours and streamlines of the flow around a cylinder with slip boundary conditions, $Re = 30$.

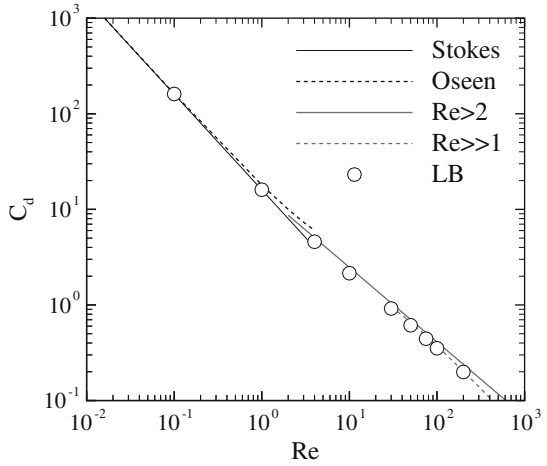


**Fig. 7.** Evolution of the drag coefficient $C_d$ as a function of the Reynolds number for a 2D circular cylinder with slip boundary conditions. LB results, and analytical and experimental expressions.

pressure isocontours are plotted. In Fig. 7 the evolution of the drag coefficient as a function of the Reynolds number obtained by numerical simulations with the LB method is plotted and compared with Eqs. (28)–(31).

## 5. Conclusions

An approach to prescribe macroscopic-gradient boundary conditions in lattice Boltzmann methods, in which finite-difference stencils are use for macroscopic variables, has been introduced and validated.

The proposal to implement velocity-gradient conditions (i.e. stresses) is similar in concept to the treatment used in immerse boundary methods for Navier–Stokes equations [47,52]. Extensions of the method, not presented here, could include boundary conditions for other variables related to velocity derivatives, such as vorticity, and also to pressure or scalar gradients. Additionally, a nonreflecting formulation of this boundary condition is possible following the characteristic approach applied in [53] for lattice Boltzmann methods.

The structure of the proposed scheme is flexible and it is applicable to the lattice Boltzmann equation with any collision operator; additionally, the interpolation scheme for curved geometries can be switched to any other if the accuracy [22] or the localness [54] need to be improved. The extension to three-dimensional flows is straightforward and it does not require further considerations.

## Acknowledgments

S.I. acknowledges support from the European Social Fund through the I3P CSIC Programme. This work was partially funded by the Spanish Government under Projects ENE2007-67217/ALT and ENE2008-06683-C03-03.

## References


[1] S. Chen, G. Doolen, Lattice Boltzmann method for fluid flows, Annu. Rev. Fluid Mech. 30 (1998) 329–364.
[2] D.A. Wolf-Gladrow, Lattice-gas cellular automata and lattice boltzmann models. An introduction, Lecture Notes in Mathematics, vol. 1725, Springer, 2000.
[3] S. Succi, The Lattice Boltzmann Equation for Fluid Dynamics and Beyond, Oxford, 2001.
[4] D. Yu, R. Mei, L.-S. Luo, W. Shyy, Viscous flow computations with the method of lattice Boltzmann equation, Prog. Aerosp. Sci. 39 (2003) 329–367.
[5] S.S. Chikatamarla, I.V. Karlin, Entropy and Galilean invariance of lattice Boltzmann theories, Phys. Rev. Lett. 97 (2006) 190601.
[6] C. Pan, L.-S. Luo, C.T. Miller, An evaluation of lattice Boltzmann schemes for porous medium flow simulation, Comput. Fluids 35 (2006) 898–909.
[7] J. Boyd, J. Buick, J.A. Cosgrove, P. Stansell, Application of the lattice Boltzmann model to simulated stenosis growth in a two-dimensional carotid artery, Phys. Med. Biol. 50 (2005) 4783–4796.
[8] C. van Treeck, E. Rank, M. Krafczyk, J. Tölke, B. Nachtwey, Extension of a hybrid thermal LBE scheme for large-eddy-simulations of turbulent convective flows, Comput. Fluids 35 (2006) 863–871.
[9] E. Fares, Unsteady flow simulation of the Ahmed reference body using a lattice Boltzmann approach, Comput. Fluids 35 (2006) 940–950.
[10] A.J.C. Ladd, Numerical simulations of particulate suspensions via a discretized Boltzmann equation. Part 2. Theoretical foundation, J. Fluid Mech. 271 (1994) 311–339.
[11] I. Ginzbourg, P. Adler, Boundary flow condition analysis for the three-dimensional lattice Boltzmann model, J. Phys. II France 4 (1994) 191–214.
[12] P.A. Skordos, Initial and boundary conditions for the lattice Boltzmann method, Phys. Rev. E 48 (1993) 4823.
[13] D.P. Ziegler, Boundary conditions for Lattice Boltzmann simulations, J. Stat. Phys. 71 (1993) 1171–1177.
[14] D.R. Noble, S. Chen, J.G. Georgiadis, R. Buckius, A consistent hydrodynamic boundary condition for lattice Boltzmann simulations, Phys. Fluids 7 (1995) 203.
[15] R. Maier, R. Bernard, D. Grunau, Boundary conditions for the lattice Boltzmann method, Phys. Fluids 8 (1996) 1788.
[16] Q. Zou, X. He, On pressure and velocity boundary conditions for the Lattice Boltzmann BGK model, Phys. Fluids 9 (1997) 1591–1598.
[17] I. Ginzbourg, D. d'Humières, Local second-order boundary method for lattice Boltzmann models, J. Stat. Phys. 84 (1996) 927–971.
[18] O. Filippova, D. Hänel, Lattice-Boltzmann simulation of gas-particle flow in filters, Comput. Fluids 26 (7) (1997) 697–712.
[19] R. Mei, L.-S. Luo, W. Shyy, An accurate curved boundary treatment in the lattice Boltzmann method, J. Comput. Phys. 155 (1999) 307.
[20] M. Bouzidi, M. Firdaouss, P. Lallemand, Momentum transfer of a Boltzmann-lattice fluid with boundaries, Phys. Fluids 13 (11) (2001) 3452–3459.
[21] I. Ginzburg, D. d'Humières, Multireflection boundary conditions for lattice Boltzmann models, Phys. Rev. E 68 (2003) 066614.
[22] I. Ginzburg, F. Verhaeghe, D. d'Humières, Two-relaxation-time lattice Boltzmann scheme: about parametrization, velocity, pressure and mixed boundary conditions, Commun. Comput. Phys. 3 (2) (2008) 427–478.
[23] H. Chen, C. Teixeira, K. Molving, Realization of fluid boundary conditions via discrete Boltzmann dynamics, Int. J. Mod. Phys. C 9 (1998) 1281–1292.
[24] M. Rohde, D. Kandhai, J.J. Derksen, H.E.A. Van den Akker, Improved bounce-back methods for no-slip walls in lattice-Boltzmann schemes: theory and simulations, Phys. Rev. E 67 (2003) 066703.
[25] R. Verberg, A.J.C. Ladd, Lattice-Boltzmann model with sub-grid-scale boundary conditions, Phys. Rev. Lett. 84 (2000) 2148–2151.
[26] S. Chen, D. Martínez, R. Mei, On boundary conditions in lattice Boltzmann methods, Phys. Fluids 8 (1996) 2527.
[27] Z. Guo, C. Zheng, B. Shi, An extrapolation method for boundary conditions in lattice Boltzmann method, Phys. Fluids 14 (6) (2002) 2007–2010.
[28] M. Junk, Z. Yang, One-point boundary condition for the lattice Boltzmann method, Phys. Rev. E 72 (2005) 066701.
[29] B. Chun, A.J.C. Ladd, Interpolated boundary condition for lattice Boltzmann simulations of flows in narrow gaps, Phys. Rev. E 75 (2007) 066705.
[30] C. Shu, N. Liu, Y. Chew, A novel immersed boundary velocity correction-lattice Boltzmann method and its application to simulate flow past a circular cylinder, J. Comput. Phys. 226 (2007) 1607–1622.
[31] M. Sbragaglia, S. Succi, Analytical calculation of slip flow in lattice Boltzmann models with kinetic boundary conditions, Phys. Fluids 17 (2005) 093602.
[32] L. Szalmás, Slip-flow boundary condition for straight walls in the lattice Boltzmann model, Phys. Rev. E 73 (2006) 066710.
[33] F. Verhaeghe, L.-S. Luo, B. Blanpain, Lattice Boltzmann modeling of microchannel flow in slip flow regime, J. Comput. Phys. 228 (1) (2009) 147–157.
[34] X. Yin, D.L. Koch, R. Verberg, Lattice-Boltzmann method for simulating spherical bubbles with no tangential stress boundary conditions, Phys. Rev. E 73 (2006) 026301.
[35] W. Miller, Flow in the driven cavity calculated by the lattice Boltzmann method, Phys. Rev. E 51 (1995) 3659–3669.
[36] S. Ansumali, I.V. Karlin, Kinetic boundary conditions in the lattice Boltzmann method, Phys. Rev. E 66 (2) (2002) 026311.
[37] D. d'Humières, Generalized lattice-Boltzmann equations, AIAA rarefied gas dynamics: theory and simulations, Prog. Astronaut. Aeronaut. 59 (1992) 450–548.
[38] Z. Guo, C. Zheng, B. Shi, Discrete lattice effects on the forcing term in the lattice Boltzmann method, Phys. Rev. E 65 (2003) 066308.
[39] P. Lallemand, L.-S. Luo, Theory of the lattice Boltzmann method: dispersion, dissipation, isotropy, Galilean invariance, and stability, Phys. Rev. E 61 (2000) 6546–6562.
[40] I. Ginzburg, Equilibrium-type and link-type lattice Boltzmann models for generic advection and anisotropic-dispersion equations, Adv. Water Resour. 28 (2005) 1171–1195.
[41] I. Ginzburg, Generic boundary conditions for lattice Boltzmann models and their application to advection and anisotropic-dispersion equations, Adv. Water Resour. 28 (2005) 1196–1216.
[42] I. Ginzburg, Variably saturated flow described with the anisotropic lattice Boltzmann methods, J. Comput. Fluids 25 (2006) 831–848.
[43] I. Ginzburg, Lattice Boltzmann modeling with discontinuous collision components. Hydrodynamic and advection–diffusion equations, J. Stat. Phys. 126 (2007) 157–203.
[44] I. Ginzburg, F. Verhaeghe, D. d'Humières, Study of simple hydrodynamic solutions with the two-relaxation-times lattice Boltzmann scheme, Commun. Comput. Phys. 3 (2008) 519–581.
[45] P.M. Gresho, Incompressible fluid dynamics: some fundamental formulation issues, Ann. Rev. Fluid Mech. 23 (1991) 413–453.
[46] S. Majumdar, G. Iaccarino, P. Durbin, RANS solvers with adaptive structured boundary non-conforming grids, Annual Research Briefs, Center for Turbulence Research, 2001, pp. 353–366.
[47] G. Kalitzin, G. Iaccarino, Toward immerse boundary simulation of high Reynolds number flows, Annual Research Briefs, Center for Turbulent Research, 2003, pp. 369–378.
[48] U. Piomelli, E. Balaras, Wall-layer models for large-eddy simulations, Ann. Rev. Fluid Mech. 34 (2002) 349.
[49] Z. Guo, T.S. Zhao, Y. Shi, Physical symmetry, spatial accuracy, and relaxation time of the lattice Boltzmann equation for microgas flow, J. Appl. Phys. 99 (2006) 074903.
[50] J. Crank, The Mathematics of Diffusion, second ed., Oxford University Press, 1975.
[51] R. Clift, J. Grace, M. Weber, Bubbles, Drops and Particles, Academic Press, 1978.
[52] R. Mittal, G. Iaccarino, Immersed boundary methods, Annu. Rev. Fluid Mech. 37 (2005) 239–261.
[53] S. Izquierdo, N. Fueyo, Characteristic nonreflecting boundary conditions for open boundaries in lattice Boltzmann methods, Phys. Rev. E 78 (2008) 046707.
[54] M. Junk, A. Klar, L.-S. Luo, Asymptotic analysis of the lattice Boltzmann equation, J. Comput. Phys. 210 (2005) 676–704.